Commissioning and performance of TITAN's Multiple-Reflection Time-of-Flight Mass-Spectrometer and isobar separator

Citation for published version:
for the TITAN collaboration 2021, 'Commissioning and performance of TITAN's Multiple-Reflection Time-of-Flight Mass-Spectrometer and isobar separator', *Nuclear Instruments and Methods in Physics Research Section A: Accelerators, Spectrometers, Detectors and Associated Equipment*, vol. 1018, 165823, pp. 1-14. https://doi.org/10.1016/j.nima.2021.165823

Digital Object Identifier (DOI):
10.1016/j.nima.2021.165823

Published In:
Nuclear Instruments and Methods in Physics Research Section A: Accelerators, Spectrometers, Detectors and Associated Equipment

Commissioning and Performance of TITAN's Multiple-Reflection Time-of-Flight Mass-Spectrometer and Isobar Separator

M. P. Reiter[a,b,c,*], S. Ayet San Andrés[a,d], J. Bergmann[a], T. Dickel[a,d], J. Dilling[b,e], A. Jacobs[b,e], A.A. Kwiatkowski[b,f], W.R. Plaß[a,d], C. Scheidenberger[a,d], D. Short[b,g], C. Will[a], C. Babcock[b], E. Dunling[b,i], A. Finlay[b,e], C. Hornung[a,d], C. Jesch[a], R. Klawitter[j], B. Kootte[b,l], D. Lascar[b,k], E. Leistenschneider[b,e], T. Murböck[b], S.F. Paul[h,b], M. Yavor[l], for the TITAN Collaboration[b]

[a] *II. Physikalisches Institut, Justus-Liebig-Universität, 35392 Gießen, Germany*
[b] *TRIUMF, 4004 Wesbrook Mall, Vancouver, British Columbia V6T 2A3, Canada*
[c] *Insitute for Particle and Nuclear Physics, The University of Edinburgh, EH9 3FD Edinburgh, United Kingdome*
[d] *GSI Helmholtzzentrum für Schwerionenforschung GmbH, Planckstraße 1, 64291 Darmstadt, Germany*
[e] *Department of Physics & Astronomy, University of British Columbia, Vancouver, British Columbia V6T 1Z1, Canada*
[f] *Department of Physics and Astronomy, University of Victoria, Victoria, British Columbia V8P 5C2, Canada*
[g] *Department of Chemistry, Simon Fraser University, Burnaby, British Columbia V5A 1S6, Canada*
[h] *Ruprecht-Karls-Universität Heidelberg, D-69117 Heidelberg, Germany*
[i] *Department of Physics, University of York, York, YO10 5DD, United Kingdom*
[j] *Max-Planck-Institut für Kernphysik, Heidelberg D-69117, Germany*
[k] *Center for Fundamental Physics, Northwestern University, Evanston, IL 60208, USA*
[l] *Institute for Analytical Instrumentation, Russian Academy of Sciences, 190103, St. Petersburg, Russia*

Abstract

TRIUMF's Ion Trap for Atomic and Nuclear science (TITAN) has specialized in fast Penning Trap mass spectrometry of very short-lived radioactive isotopes. The facility has been upgraded with a Multiple-Reflection Time-of-Flight Mass Spectrometer (MR-TOF-MS) to continue its quest towards more exotic nuclides, which are critical for our understanding of nuclear structure effects far from the valley of beta stability and for the nucleosynthesis of heavy elements in explosive astrophysical environments. In this publication, we discuss the implementation, operation and performance of TITAN's MR-TOF-MS as a stand-alone high-precision mass spectrometer and as an isobar separator. By using the novel mass-selective re-trapping technique for the isobar separation, the MR-TOF-MS can consecutively perform separation and mass measurement of the same ion population, acting as its own isobar separator. The device boosts the dynamic range and reach of the TITAN facility by several orders of magnitude. The MR-TOF-MS reaches a high mass resolving power ($m/\Delta m \sim 400\,000$), high precision and mass accuracy ($\delta m/m < 10^{-7}$), is fast (common cycle time 20 ms), shows high sensitivity and very large dynamic range (ion of interest to contaminant ratios of up to 1 to 10^6).

1. Introduction

Mass spectrometry has been closely entangled with nuclear physics research since the early days of the field [1]. The highest precisions and resolving powers are typically reached with Penning Traps, which have matured into a standard of the field [2, 3]. One of these is TRIUMF's Ion Trap for Atomic and Nuclear science (TITAN) [4], which has specialized in measurements of very short-lived radioactive isotopes [5, 6]. Mass measurements of the most exotic nuclides at the outskirts of the nuclear chart play an important role in shaping our understanding of the nucleus [7], a complex quantum system of protons and neutrons, and give vital inputs for understanding the nucleosynthesis in explosive astrophysical environments [8]. Despite their success, many Penning Trap mass spectrometers at radioactive ion beam (RIB) facilities suffer from strong isobaric background, produced simultaneously with the minute amounts of the isotope of interest [9].

In the last decade a new type of spectrometer, so-called Multiple-Reflection Time-of-Flight Mass Spectrometer (MR-TOF-MS), has been brought into routine operation. In these time-of-flight mass spectrometers [10, 11] long flight paths and therefore high resolving powers can be achieved by storing ions between two electrostatic ion mirrors [12]. Due to their unique combination of performance parameters, being (i) high mass resolving power ($m/\Delta m \sim 10^5$), (ii) high precision and mass accuracy ($\delta m/m \sim 10^{-7}$), (iii) fast measurement cycle ($\sim$ tens of ms), (iv) single ion sensitivity and (v) strong background handling capabilities (common ion of interest to contaminant ratios of up to 1 to 10^4), these devices are well suited for mass measurements of the most exotic isotopes [13]. In addition, they can provide isobar separation for Penning Traps and are today employed at many RIB facilities [14, 15, 16, 17, 18]. They have led to breakthroughs in nuclear astrophysics [19, 20, 21] and many aspects of nuclear structure research: (i) the evolution of the exotic $N = 32$ neutron shell [22, 23, 24, 25, 26], (ii) helped towards a better understanding of actinides [27, 28], (iii) superheavy elements [29] and (iv) the study of isomers [30, 31, 32],

*Corresponding author: mreiter@ed.ac.uk

to name a few.

The TITAN Multiple-Reflection Time-of-Flight Mass Spectrometer (MR-TOF-MS) and Isobar Separator has been developed at the Justus Liebig University Giessen [33] and its design and initial offline performance have been described in [34]. In this paper we discuss the implementation, commissioning and online operation of the device. Further we showcase its current performance, including recent upgrades to the system described in [35], in terms of efficiency, mass resolving power, mass accuracy and precision as well as its unique isobar separation capabilities.

2. Experimental Facilities

2.1. The TITAN Facility

TRIUMF's Ion Trap for Atomic and Nuclear science [4] is located at the Isotope Separator and Accelerator (ISAC) facility [36, 37], TRIUMF, Vancouver, Canada. It is a multiple ion trap system specialized in performing high-precision mass measurements and in-trap decay spectroscopy of short-lived radioactive isotopes. At ISAC radioactive isotopes are produced via the ISOL method by impinging an intense 10 – 100 μA 480 MeV proton beam onto a variety of production targets [38]. Isotopes are produced via nuclear reactions inside the target, diffuse towards an ion source and are formed into a low-energy radioactive ion beam (RIB) with 20 – 40 keV energy. The continuous cocktail beam is mass separated by ISAC's magnetic dipole separator with a mass resolving power of about 2000 [39] and transported to TITAN. Here the ions are first captured, cooled and bunched in a helium gas-filled Radio Frequency Quadrupole (RFQ) Cooler & Buncher [40], shown in Fig. 1.

Following the RFQ Cooler & Buncher the kinetic energy of emerging ion bunches can be adjusted using a pulsed drift tube and typical beam transport energies across the TITAN platform are between 1.4 and 2 keV. Along the TITAN beam line several Faraday Cups and microchannel plate (MCP) detectors are positioned to monitor the beam transport. The trapping and ejection voltages of the TITAN RFQ Cooler & Buncher are optimized to ensure minimal energy spread (roughly 5 – 8 eV) suitable for direct injection into a Penning Trap mass spectrometer using Lorentz steerers [41]. As a consequence of the shallow ejection field strength at the trapping segment, the temporal spread of the ion bunch is dominated by the turn-around time and bunches with a width of about < 1 μs are sent to the individual ion traps at TITAN, see Fig. 1a for a typical bunch profile at MCP 0. The precision Measurement Penning Trap system (MPET) is used for mass measurements requiring relative precisions $\delta m/m < 10^{-8}$ [42]. An Electron Beam Ion Trap (EBIT) [43] can be used for charge breeding producing highly-charged ions (HCI), for in-trap decay spectroscopy of HCI [44] or for the capture of daughter nuclei following nuclear decays [45]. The use of HCI boosts the precision and resolving power of MPET and is particular suitable for heavy and short-lived species [46]. As MPET has been designed to fully leverage HCI it is not equipped with a gas-filled preparation trap.

Despite the success, many measurements at TITAN suffer from a strong isobaric background, distinct to the ISOL method of beam production. This background often prevents high precision measurement of the most exotic species of interest [47, 48]. To overcome this limitation an isobar separator based on the MR-TOF-MS technique was developed at the Justus Liebig University Giessen [33, 34] and has been installed at TITAN. The device is based on the design of the MR-TOF-MS devices in operation at the FRS Ion Catcher [16, 49] at GSI, Germany and for analytical mass spectrometry [50] at the University of Giessen.

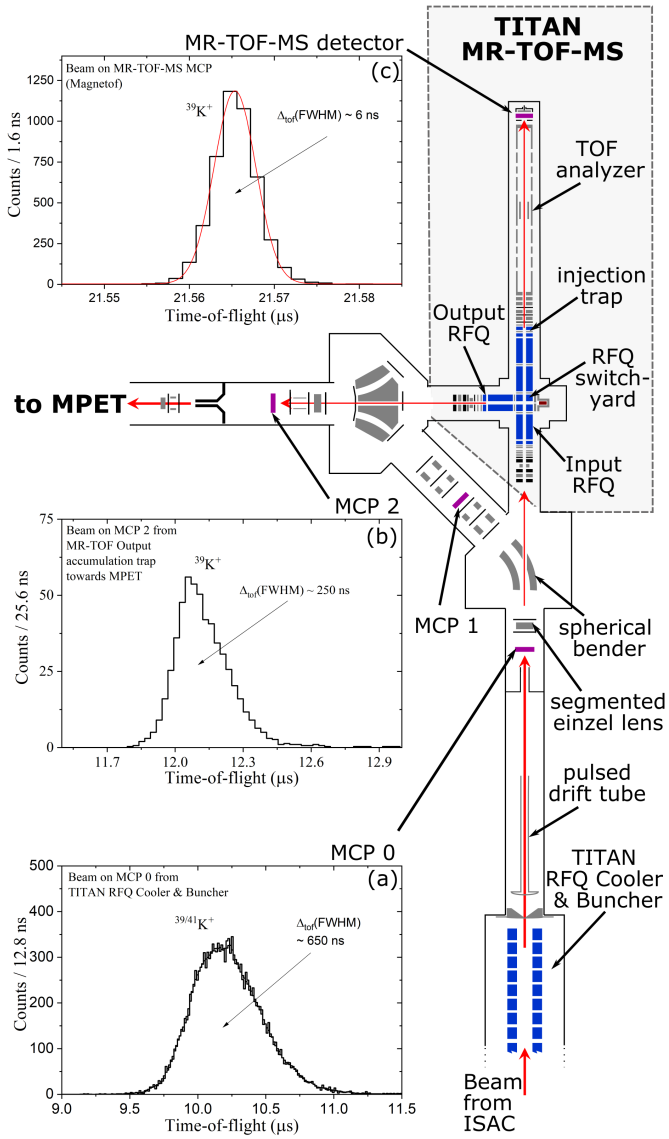

Figure 1: Schematic layout of the beam transport from the TITAN RFQ Cooler & Buncher into the MR-TOF-MS and towards the Measurement Penning Trap (MPET) and Electron Beam Ion Trap (EBIT). Typical ion bunch profiles are shown at several locations (MCP 0, MCP 2, MR-TOF-MS detector).

2.2. The TITAN MR-TOF-MS

In general, the time-of-flight technique relies on the non-relativistic relation between the mass m and charge q of an ion and its time-of-flight t_{tof} needed to travel a certain flight path l

through the effective electric potential $U_{\mathrm{eff}}(l)$:

$$\frac{m}{q} = \frac{2U_{\mathrm{eff}}(l)}{l^2} t_{\mathrm{tof}}^2 \tag{1}$$

The real time of flight t_{tof} is shifted from the measured time of flight t_{exp} due to signal propagation times and electronic delays, which are constant for a given experiment and data acquisition system, resulting in the calibration function of

$$\frac{m}{q} = a(t_{\mathrm{exp}} - t_0)^2 \tag{2}$$

with parameter a being a device-specific calibration parameter. The latter depends on the kinetic energy of the ions and the effective path length given by the geometrical path and the voltages applied to the electrode system. The time offset t_0 can be determined offline from a dedicated measurement of the time-of-flight and known mass-to-charge ratio of stable calibration ion species. The calibration parameter a is determined online using a well-known reference ion species present in the radioactive beam.

The mass resolving power can be linked to the total time-of-flight t_{tof} and the full width half maximum (FWHM) of the time-of-flight distribution Δt_{tof} as

$$R = \frac{m}{\Delta m} = \frac{t_{\mathrm{tof}}}{2\Delta t_{\mathrm{tof}}}. \tag{3}$$

An elegant way to increase the resolving and separation power of the time-of-flight mass analyzer is by extending the flight paths by reflecting the ions multiple times between two electrostatic ion mirrors [12]. The total time of flight can thus be written in terms of the time to complete a single turn t_{turn}, the number of turns N and the time of flight from the starting position to the detector without any turns t_{offset}. The mass resolving power of such a multiple turn spectrometer can in general be described by

$$R = \frac{t_{\mathrm{turn}} \cdot N + t_{\mathrm{offset}}}{2\sqrt{(\Delta t_{\mathrm{turn}} \cdot N)^2 + (\Delta t_{\mathrm{offset}})^2}}, \tag{4}$$

with $\Delta t_{\mathrm{offset}}$ being the initial peak width and Δt_{turn} the increase in peak width per turn due to ion optical aberrations. At long flight path, a large number of turns, the achievable resolving power becomes independent of the initial peak width $\Delta t_{\mathrm{offset}}$ and resolving powers on the order of $m/\Delta m$ of $\sim 10^5$ can be achieved.

However, at broad initial mass distribution and high number of turns it can occur that lighter ions overtake heavier ones. Thus, the mass spectrum can become ambiguous, because ions undergo a different number of turns inside the mass analyzer. In this case eq. 1 needs to be modified in order to account for the different flight path an ion has undergone. Assuming s_{offset} being the length of the flight path from the start to the final detector without any turns and s_{turn} the length of one turn, the total flight path l of an ion can than be written as $l = s_{\mathrm{offset}} + N \cdot s_{\mathrm{turn}}$, yielding a calibration function [28] of

$$\frac{m}{q} = \frac{2U_{\mathrm{eff}}(l)}{(s_{\mathrm{offset}} + N \cdot s_{\mathrm{Turn}})^2}(t_{\mathrm{exp}} - t_0)^2. \tag{5}$$

Thich can be simplified to

$$\frac{m}{q} = \frac{c(t_{\mathrm{exp}} - t_0)^2}{(1 + N \cdot b)^2}, \tag{6}$$

with $b = s_{\mathrm{turn}}/s_{\mathrm{offset}}$ and $c = 2U_{\mathrm{eff}}(l)/s_{\mathrm{offset}}^2$. Thus a turn independent calibration, requiring three known calibration species with at least two different numbers of turns N to determine b, c and t_0, can be performed [51].

The TITAN MR-TOF-MS operates in three distinct operation modes, being:

- Mass measurement mode – After a certain number of reflections ions are guided onto a fast time-of-flight detector. There the time-of-flight and thus the mass of all ion species is measured. The mass can typically be determined to a relative precision of $\delta m/m \sim 10^{-7}$. Since the MR-TOF-MS is a non-scanning mass measurement technique, it allows a fast determination of the composition of the ISAC beam and individual yields of all species at the same time, including stable nuclides. Therefore unwanted isobaric contaminations can be detected, identified and quantified prior to the isobar separation. This procedure allows for real-time optimization of the ISAC mass separator and has been shown to improve the beam purity by about an order of magnitude compared to the initial tuning [52].

- Isobar separation mode – Compared to other MR-TOF-MS, which rely on either Bradbury-Nielsen gates [53, 54, 55, 30], selective switching of the ion mirrors [56] or drift tube [57], the TITAN MR-TOF-MS uses mass-selective re-trapping [58]. Here, the ions are directed back towards the initial RF injection trap and the ions-of-interest are selectively re-trapped by switching the injection trap quickly from a retarding potential to a trapping potential [58]. By choosing a correct moment in time, the so-called re-trapping time t_{RT}, only the ions-of-interests are at rest, while ions with a different mass-to-charge ratios arrive at the trap at different times and thus retain a significant amount of kinetic energy and therefore are not re-trapped. Making use of this operation mode, the MR-TOF-MS can provide isobarically purified beams for all downstream experiments. In addition, as the re-captured ion bunches are automatically re-cooled in the gas-filled RFQ beam line of the MR-TOF-MS there is no need for additional cooling trap right before MPET.

- Combined isobar separation and mass measurement mode – Combing both previous operation modes the TITAN MR-TOF-MS can uniquely act as its own high-resolution, high-throughput isobar separator prior to performing a mass measurement of a purified ion sample. This allows additional background suppression and increases the dynamic range of the measurement within the same device by several orders of magnitude. In addition, this mode allows for fast and reliable tuning of the isobar separation and optimization of the beam composition for the downstream ion traps.

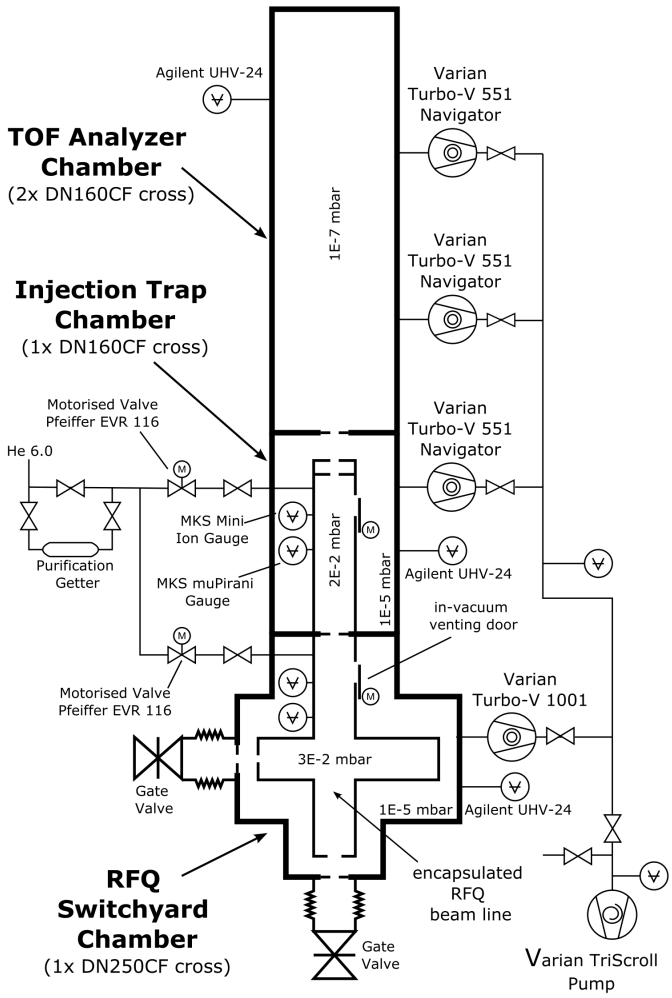

Figure 2: Schematic layout of the vacuum system of the TITAN MR-TOF-MS. The gas handling system as well as the location of the two gas inlets, one close to the RFQ switchyard and one close to the injection trap, are shown. Typical pressures during operation are indicated in the individual vacuum chambers.

The TITAN MR-TOF-MS has been designed to ensure minimal impact on the existing facility and to fit the limited floor space available on the TITAN platform [34]. It was installed on top of the vertical RFQ Cooler & Buncher between two 45 degree spherical bender sections. As such, it can be bypassed without affecting the beam transport to the MPET and EBIT ion traps. Ions can be sent to the MR-TOF-MS through a 8 mm hole introduced in the outer electrode of the lower spherical bender, as shown in Fig. 1. To further ensure efficient beam transport into the MR-TOF-MS a new fourfold segmented einzel lens was installed before the bender. The new steering and lensing capabilities also improved the transmission to the MPET and EBIT ion traps. In order to monitor the beam transport into the MR-TOF-MS a new MCP detector, referred to as MCP 0 in Fig. 1 was installed between the RFQ Cooler & Buncher and the lower spherical bender.

The TITAN MR-TOF-MS consists of an helium gas-filled low-energy RFQ based beam transport system and a vacuum time-of-flight analyzer. The gas-filled RFQs are encapsulated for differential pumping. The ion optical elements are housed in one DN250CF and three DN160CF vacuum crosses, pumped by one 1000 l/s and three 550 l/s turbomolecular pumps (Varian Turbo-V 1001 & 551 Navigator). A schematic layout of the vacuum system is shown in Fig. 2. The device can be separated from the preexisting TITAN beam line by two isolation valves. Each vacuum chamber is equipped with a cold cathode vacuum gauge (Agilent UHV-24). A base pressure of $< 2 \times 10^{-8}$ mbar is achieved in all chambers prior to applying helium gas to the system.

During operation the encapsulated RFQ system is kept at a gas pressure of about $\approx 2 \times 10^{-2}$ mbar He. Two gas inlets, one at the RFQ switchyard chamber and one at the injection trap chamber supply the system with getter (CHROMSPEC^{TM} 750cc Trap) purified He gas (Praxair 6.0RS). The pressure inside the encapsulation is directly monitored using vacuum-compatible pressure gauges mounted within the system (MKS MIG and MKS MicroPirani), whereas the gas flow is controlled by motorized regulation valves (Pfeiffer EVR 116) [33]. The encapsulation has been equipped with in-vacuum venting doors, which allow reduced evacuation times and improved cleanliness after pumping of the device [59]. Opening the in-vacuum venting doors, the encapsulation can be evacuated to $\approx 2 \times 10^{-7}$ mbar before allowing helium gas into the system.

2.2.1. The Transport RFQ System

The RFQ transport system is based on the design of the RFQs of the MR-TOF-MS at the FRS Ion catcher at GSI, Germany [60, 61]. It relies on encapsulated round RFQs (inner / field diameter of 10 mm, rod diameter of 13 mm) made out of resistive plastic rods (resistance of $\approx 5\ \Omega$/cm) to create axial drag fields in addition to radial confinement [16]. Apertures between individual resistive RFQ segments can be used to store ions, which enables versatile ion manipulation options. An RFQ switchyard [49] is located at the heart of the transport system. It allows transport of ions towards and from all directions of the switchyard as well as merging of the radioactive ions-of-interest with stable calibration species from a thermal ion source (Heatwave #101139). In addition, a Channeltron detector (PHOTONIS MAGNUM^{TM}) is mounted on one side of the switchyard and can be used to monitor the total beam intensity. At the top of the transport system a dedicated injection trap system is positioned. It consists of a preparation trap segment and a separate injection trap. The former allows accumulation and pre-cooling of ion populations while the latter provides optimal ion bunch properties for the time-of-flight analyzer. The complete low energy transport system is biased to slightly above 1.3 kV, as the injection trap is fixed at 1.3 kV. All high voltages are supplied from ISEG EHS standard modules directly, whereas the voltage drop along the restive RFQ segments are produced by Wiener low voltage power supplies, housed and biased to 1.3 kV in a dedicated high voltage cage. Sinusoidal radio frequency signals for the RF structures are provided by in-house built resonant drivers [51] operating at 1.1 MHz, 1.5 MHz and 1.6 MHz supplying the RFQ beam line, the RFQ switchyard and the injection trap separately.

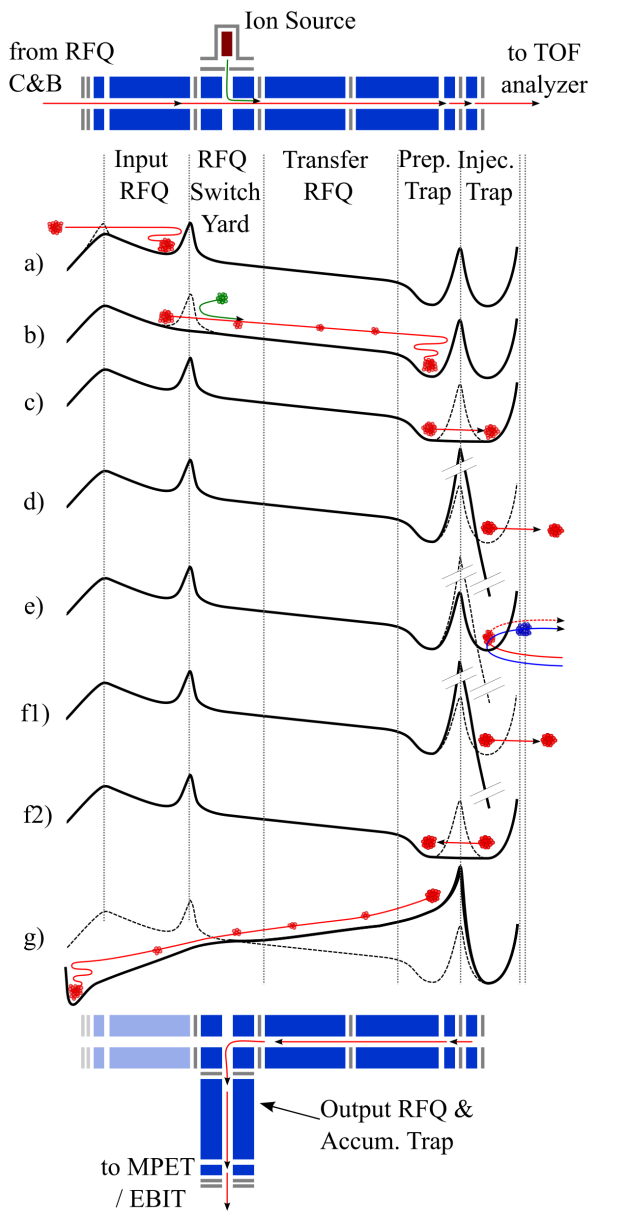

Figure 3: Schematic figure (not to scale) of the operation principle of the TITAN MR-TOF-MS showing schematic electric potential (solid line) along the RFQ transport system. The potential of the previous step is indicated by the dashed line. Movement of ions during one MR-TOF-MS cycle is indicated. a) Capture of an ion bunch in the Input RFQ. b) Transported along the internal RFQ transport system to the preparation trap. In the RFQ switchyard calibration ions can be merged with the RIB. c) Transport from the preparation trap to injection trap. d) Injection into the time-of-flight analyzer for isobar separation or mass measurement. e) Mass-selective re-trapping of the ions-of-interest in the injection trap. f1) Second injection of a purified ion bunch into the analyzer for consecutive mass measurement. f2) Transport backwards to the preparation trap. g) Transport to an accumulation trap segment at the end of the output RFQ. Step a) to f2) are in relation to the top ion optics schematic, whereas step g) relates to the bottom schematic. (For details see text.)

To ensure efficient and fast transport through the internal RFQ beam line axial drag fields of about 0.5 – 0.7 V/cm are applied along the resistive RFQ rods. Estimated pseudopotentials between 5 – 20 eV have been shown to provide sufficient radial confinement to capture and transport ion bunches from the TITAN RFQ Cooler & Buncher.

The transport inside the MR-TOF-MS is performed stepwise and a schematic of the ion transport scheme is shown in Fig. 3. Ions enter the gas-filled region through a matching section, which focusses and steers the ion beam through a 2 mm differential pumping aperture. The aperture is additionally used as an ion gate, switched between 1500 V (blocking) and 1350 V (open), to only allow ions of a certain mass-over-charge range to enter the system. Ions are captured with a minimal amount of kinetic energy (Fig. 3: step a) by matching the kinetic energy of the ions from the RFQ Cooler & Buncher to the entrance potential of the Input RFQ (1340 V). Ions are cooled and accumulated for about ≈ 1 ms in front of the RFQ switchyard, before being transported to the preparation trap, see Fig. 3 top schematic for a detailed layout of the ion optical elements. In addition, calibration ion species from the internal surface ion source can be merged with the radioactive beam (Fig. 3: step b). At the preparation trap ions are pre-cooled for ≈ 2 ms and then, by lowering the potential of the aperture between the preparation trap and the injection trap for a short period of time (8 μs for $^{133}Cs^{+}$), transferred between the two traps with minimal heating (step c). The injection trap segment has been designed to ensure symmetric radial and axial confinement, typically about 15 V trapping depth, as well as strong and homogeneous ejection fields, typically in the order of 80 V/mm [50]. The ejection field is generated by the apertures surrounding the injection trap being switched in a push-pull configuration. As a result of the high extraction field strength a reduced turn-around time is achieved and ion bunches with narrow time-of-flight spread of around 6 ns for $^{39}K^{+}$, as shown in Fig. 1c, are formed and injection into the time-of-flight analyzer (step d). The ion bunches have a mean kinetic energy of 1300 eV. The energy spread was estimated to be about 17 eV (1.3%) based on simulations.

In isobar separation mode, following a re-trapping operation, the purified sample is re-cooled for 3 to 5 ms and then either injected into the mass analyzer for a second time-of-flight analysis (step f1) or transported backwards to the preparation trap (step f2). Raising the potential of the preparation trap and inverting the gradient along the transfer RFQ and RFQ switchyard elements guides the pure sample towards the output RFQ (step g), see Fig. 3 bottom schematic for a detailed layout of the ion optical elements. Here, in an additional trapping segment several purified ion bunches can be accumulated before being sent to the downstream experimental stations, effectively decoupling the MR-TOF-MS cycle time from the typically longer cycle of the Measurement Penning Trap MPET or EBIT. In Fig. 1b a typical ion bunch of purified $^{39}K^{+}$ from the output accumulation trap is shown.

2.2.2. *The Time-of-Flight Analyzer*

The ion bunches ejected from the injection trap fly through a double aperture, which serves as a differential pumping barrier, and an x-y-steerer - einzel lens combination towards the time-of-flight analyzer. The ion optical design and properties of the analyzer are based on [16, 62] and have been described in detail in [62]. However, to follow height restrictions in the

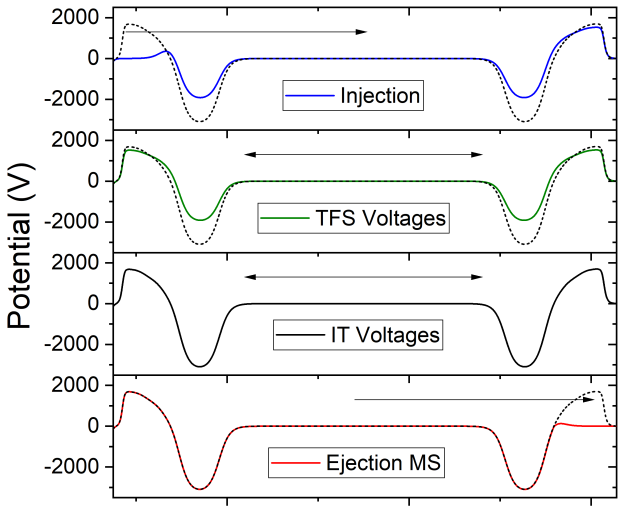

Figure 4: Schematic of the electric potentials applied to the time-of-flight analyzer. The potentials applied during isochronous turns (IT) is shown in comparison to the potentials applied during ion injection, time focus shift (TFS) turn [63] and ejection towards the time-of-flight detector. The mean kinetic energy of the ions is indicated by the height of the black arrow. It remains constant during all depicted steps.

ISAC I experimental hall, the TITAN MR-TOF-MS analyzer has been scaled to a length of about 500 mm, resulting in an ion mirror as in [50]. It consists of two sets of four cylindrical electrodes, forming two opposing ion mirrors, separated by a grounded drift tube. At the center of the drift tube a four fold deflector is mounted. It can be used for beam alignment during the injection and first passing of ion bunches or as a mass range selector (MRS) to remove out unwanted ions with a different mass number compared to the ions of interest. At the top of the analyzer structure an isochronous single ion detector (ETP MagneTOF™) is mounted and the ion's time-of-flight is measured using a time-to-digital converter (FAST ComTec MCS6A-5T8) [35].

The time-of-flight focus is aligned using the dynamic time-focus shift (TFS) method [63]. The ion optical properties of the electrostatic mirrors have been optimized such that every turn, following the initial TFS turn, is isochronous. In the following these are referred to as isochronous turns (IT). This creates an intermediate (virtual) time-of-flight focus after every full IT in front of the injection trap and at the detector, for additional details of the scheme see [63]. Thus, in eq. 4 t_{turn} and t_{offset} can be replaced with t_{IT} and t_{TFS} (the time from the injection trap through the TFS turn to the detector), respectively, resulting in

$$R = \frac{t_{\mathrm{IT}} \cdot N + t_{\mathrm{TFS}}}{2\sqrt{(\Delta t_{\mathrm{IT}} \cdot N)^2 + (\Delta t_{\mathrm{TFS}})^2}} \tag{7}$$

with Δt_{TFS} representing the achievable peak width after only one TFS turn and Δt_{IT} the peak broadening per number of IT.

To perform the dynamic time focus shift different electric potentials are applied to the ion mirrors during the first turn. The potential on axis is schematically shown in Fig. 4. As such, three level switching of the mirror potentials (Injection/Ejection, TFS and IT) are required.

Switching of the ion mirrors for injection and ejection [13] in combination with the TFS method enables a time focus simultaneously at the detector during mass measurement mode and at the correct place in front of the injection trap during isobar separation mode. The TFS method enables the high extraction field strength at the injection trap and, as such, the formation of very narrow time-of-flight ion bunches. As such, the scheme allows simultaneously high mass resolving powers and independent turn numbers in both operation modes, thereby making the operation of the device highly flexible and allowing for a fast change of settings. In addition the resolving power at a given number of IT is automatically maximized and no re-tuning for different numbers of turns is needed [13].

To ensure minimal impact on the ions inside the analyzer, switching of the mirror potentials from one state to another is performed at the moment in time when the ions of interest are in the opposing ion mirror. The mirror potentials are provided by ISEG EHS high precision modules and are additionally stabilized using passive RC filters with a cut off frequency of ~ 1.6 Hz [35]. Precise and reproducible switching is achieved via home-built high voltage switches [51], which in addition enable the required three level switching. The timings of the device are controlled by an in-house written control and measurement software, described in [35].

The TITAN MR-TOF-MS is operated at a fixed repetition rate independent of the chosen number of IT and time-of-flight of a given measurement. Typically a repetition rate of 50 Hz, 20 ms cycle time, is used, but for specific experiments repetition rates between 20 and 100 Hz have been employed. To account for the two different operation ion optical modes of the device, the common 20 ms cycle is divided into two alternating 10 ms sub-cycles for isobar separation and mass measurement. Thus, maximal time-of-flights of about ~ 9 ms are possible in each mode. In case no isobar separation is needed, ions are simply stored for the full 10 ms in the injection trap, while the potentials of the time-of-flight analyzer are switched normally. This fixed duty cycle improves the stability and reproducibility of the mirror potentials and ultimately enables the high resolving power of the device in both modes. Further, it makes the TITAN MR-TOF-MS very flexible to set up during online experiments as changing the number of IT does not change the load and duty cycle seen by the individual power supplies.

3. Performance in Mass Measurement Mode

After its installation, the TITAN MR-TOF-MS was commissioned online using stable beams from ISAC's OLIS ion source [64]. Ion beams of stable argon and neon, but also various molecules, were delivered to TITAN with beam intensities between 1 pps and 10^7pps from a plasma ion source. In addition, a surface ion source provided beams of sodium, potassium, rubidium and cesium for systematic investigations of the performance of the MR-TOF-MS.

3.1. Efficiency

A key to performing mass measurements of the most exotic species produced at ISAC are a high efficiency and sensitivity. Ions can be lost at various stages during the transport: during the initial capture and accumulation in the TITAN Cooler & Buncher, during transport and injection into the MR-TOF-MS, along the internal RFQ beam line, during the long flight path inside the time-of-flight mass analyzer or during the final detection. Making use of the different detectors along the beam line the individual losses were quantified using stable beams.

The transmission efficiency of the TITAN RFQ Cooler & Buncher has been reported elsewhere [40]. It depends on the used ISAC ion source and properties of the radioactive beam tuned to TITAN. The TITAN RFQ Cooler & Buncher is operated with a square-wave RF, which ensures a high efficiency for all mass ranges. Typical efficiencies in bunch mode are between 50 – 80%.

The capture and transport efficiency through the TITAN MR-TOF-MS internal RFQ beam line depends on the kinetic energy and phase space of the incoming ion bunches as well as on the achievable Mathieu parameters (q-values) and pseudopotentials of the RFQ system. The RF system is based on resonance circuits, which limits the mass-to-charge range of the device at a given resonance frequency. For light ion species the inductors of the RLC circuits need to be exchanged manually to increase the resonance frequency and ensure efficient transport. The capture and transport efficiency was estimated by comparing the ion count rate at the MagneTOF^{TM} detector of ions undergoing only one TFS turn compared to the rate at MCP 0, see Fig. 1 for the location of the detectors. To maximise the detection efficiency of the MCP detector, ion bunches with a kinetic energy of 20 keV were sent to the MCP. Using ion bunches with a kinetic energy of 1.36 – 1.45 keV maximised the capture in the input RFQ of the MR-TOF-MS and the detected rate at the MagneTOF^{TM} detector. The transport along the internal beam line was optimized varying the drag fields along the RFQ segments, the potential of apertures as well as the helium gas pressure and RF voltages. Under standard RF frequencies, capture and transport efficiencies between 60 – 80% were achieved for $^{39}K^+$, $^{85}Rb^+$ and $^{133}Cs^+$ and around 40% for $^{23}Na^+$ by only adjusting the RF amplitudes.

Due to the confinement in the RFQ system, ions can be stored with minimal losses for several seconds at various locations in the RFQ beam line, allowing, e.g. half-life measurements via ion counting [65, 66, 67] or accumulation of purified samples [53]. However, due to trace amounts of impurities present in the He buffer gas of the system, noble gas ions may charge exchange whereas chemical reactive species may from adducts. Storage times have been investigated during the commissioning, the results are shown in Fig. 5. A storage time of $t_{1/2} \approx 20$ ms was reached for $^{40}Ar^+$ and $t_{1/2} \approx 30$ ms for $^{22}Ne^+$, in comparison to $t_{1/2} \approx 10$ s for $^{23}Na^+$ ions. The difference in storage time between Ar and Ne ions was not further investigated but may be due to temperature changes in the ISAC experimental hall. In order to minimize possible losses due to charge-exchange, chemical reactions or decay, the RFQ beam line was optimized such that all ions are transported to the TOF detector within a single MR-TOF-MS cycle. It can be concluded, that in the standard cycle time of 20 ms the transmission for noble gasses and very chemical reactive ion species may be ~ 50% lower compared to alkali ions.

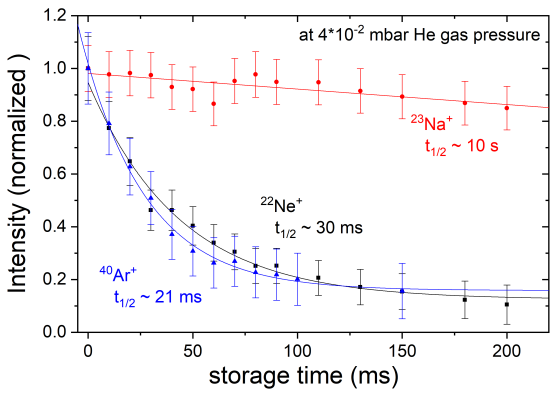

Figure 5: Storage time measurement of Ar, Ne and Na ions at the preparation trap of the MR-TOF-MS RFQ system. For noble gas species, storage times $t_{1/2} \approx 20 - 30$ ms can be achieved. Alkali-ions can be stored for up to several seconds, as shown for Na.

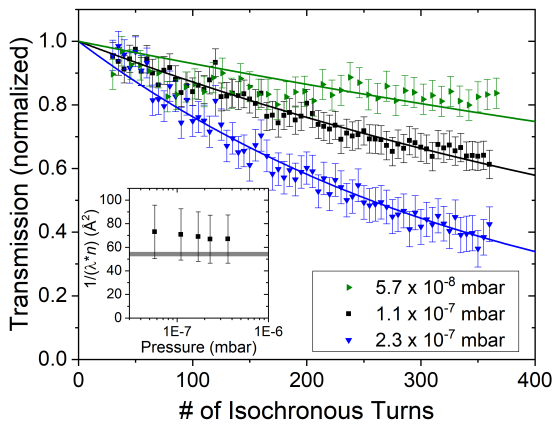

Figure 6: Transmission efficiency of the time-of-flight mass analyzer for $^{39}K^+$ as a function of the number of isochronous turns measured for different residual gas pressures, normalized to the count rate of ions undergoing one TFS turn only. Under typical residual gas conditions of $< 1 \times 10^{-7}$ mbar about ~ 60% of the ions can be detected after 350 isochronous turns. The inset shows the obtained collision cross section for potassium ions in helium gas for different pressures. The constant behavior suggest losses are dominated by collisions with residual gas atoms [50].

For the TITAN MR-TOF-MS losses in the time-of-flight analyzer mainly occur due to collisions with residual gas. Therefore, they depend on the residual gas pressure in the analyzer region, which during operation is dominated by helium gas from the injection trap. The transmission through the time-of-flight analyzer has been investigated using $^{39}K^+$ ions at different residual gas pressures, see Fig. 6. The ion intensity was kept constant, stable within about 10%, and the number of isochronous turns (IT) was increased while monitoring the

Table 1: Individual transport efficiencies for a high precision mass measurement with the TITAN MR-TOF-MS as determined during the commissioning of the device.

	Efficiency (%)
TITAN C&B	50 – 80 (bunched)
MR-TOF-MS	
Capture & RFQ beam line	60 – 80
Time of flight analyzer	~ 60 (at 350 IT)
Detection (MagneTOF™)	60 – 80
Total MR-TOF-MS	≈ 30
TITAN C&B + MR-TOF-MS	≈ 15

detected $^{39}K^+$ intensity. For this measurement the MR-TOF-MS was set to a 100 Hz repetition rate in order to allow for reduced overall measurement time. The intensity can be well described by a single exponential decay. At residual gas pressures of 2.3×10^{-7} mbar He the intensity decays with a decay constant of 256 ± 25 turns to half the initial intensity. From the fitted decay constant the collision cross section σ for potassium ions in helium can be calculated via $\sigma = (n \times \lambda)^{-1}$, with n being the particle number density and λ the corresponding mean free path obtained from the transmission loss. The inset in Fig. 6 show the cross section at different pressures. Our result is in agreement with an analytical collision cross section of 54.1 Å^2. In addition, the collision cross section is independent of the gas pressure, which suggest that the transmission losses are dominated by collisions with residual gas atoms, see discussion in [50]. During the recent upgrade of the MR-TOF-MS [35] the pumping speed at the analyzer section was increased resulting in improved residual gas pressure below $< 1 \times 10^{-7}$ mbar. As a result, losses in the time-of-flight analyzer were decreased to a decay constant of 954 ± 60 turns at 5.7×10^{-8} mbar He, which corresponds to a path length of close to 900 m.

Therefore, at typical operational pressures between $0.5 - 1 \times 10^{-7}$ mbar about 60 – 80% of the ions are transported through the time-of-flight analyzer during mass measurements utilizing high numbers of isochronous turns.

The detection efficiency of the MR-TOF-MS MagneTOF™ detector itself was estimated to lie between 60 – 80%, in line with manufacturer specifications.

The individual efficiencies are summarised in Tab. 1. A resulting efficiency of about ≈ 30% is reached with the TITAN MR-TOF-MS for high resolution mass measurements. The total efficiency for experiments is estimated with about ≈ 15%. This value is in agreement with total efficiencies determined during online radioactive beam experiments of short lived isotopes ranging between 5 to 20% determined against the ISAC Yield station [68] and calibrated Channeltron detectors in the ISAC beam line.

3.2. Mass Resolving Power

Due to the nature of the ISOL production method many different nuclides / isobars are produced and delivered to TITAN at the same time. In this case a sufficiently high mass resolving power is needed to separate the isotope of interest from other contaminant ion species.

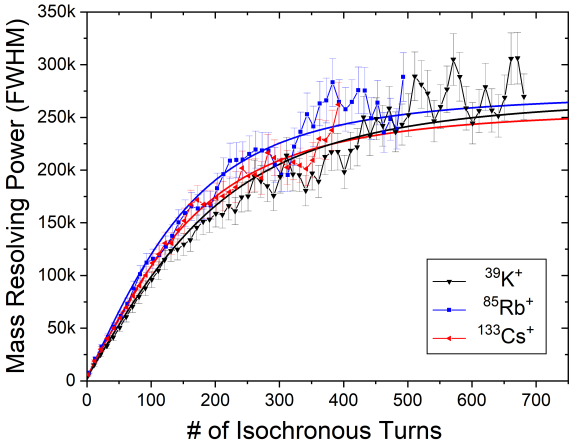

Figure 7: Mass resolving power (FWHM) measured for $^{39}K^+$, $^{85}Rb^+$ and $^{133}Cs^+$ ions as a function of the number of isochronous turns. Each turn setting was accumulated for 1000 individual MR-TOF cycles, corresponding to a 20 s accumulation time. The measurements were performed within 20 minutes from each other, no re-tuning of the time-of-flight analyzer was performed. The trapping potentials of the injection trap were adjusted to ensure proper confinement and performance for the three different species. Mass resolving powers exceeding 250 000 were reached for all species. The solid curves show fits with eq. 7 (For details see text.)

The TITAN MR-TOF-MS has been shown to reach mass resolving powers exceeding 200 000 during the first online experiments [24, 25, 21]. To optimize the system for highest mass resolving power first the initial peak width was optimized. Ions were sent to the MagneTOF™ detector after undergoing only a TFS turn and the voltages of the injection trap and the TFS turn were optimized to produce a narrow time focus at the detector. Narrow peak widths of about 6 ns for $^{39}K^+$, as shown in Fig. 1c, were reached. Then the number of IT was gradually increased and the voltages applied during the IT turns were fine-tuned to ensure minimal peak broadening. The voltages applied to the outer most mirror electrodes show the largest impact on the final peak width. To quantify the performance after the optimization, the resolving power was measured for $^{39}K^+$, $^{85}Rb^+$ and $^{133}Cs^+$ as a function of isochronous turns, see Fig 7.

The time-of-flight analyzer was not re-tuned for each species or number of IT and all scans were performed within 20 minutes. However, the parameters of the injection trap were adjusted to ensure proper ion confinement by adjusting the RF amplitude applied to the trap for the different masses. To account for effects arising from the limited rise time of the ejection potentials of the injection trap, an asymmetric axial storage potential was used to fine adjust the kinetic energy of the ions to match the energy acceptance of the time-of-flight analyzer. Preparing ion bunches in a slightly asymmetric potential shifts the position of the potential minimum along the central axis of the trap, which translates into a slightly different mean kinetic energy of the bunches once the extraction fields are applied. Based on simulations an asymmetry of the trapping potential of 1 V results in a change of the mean kinetic energy by 3.6 eV.

For each species the intensity was adjusted to about 1 de-

tected ion per MR-TOF-MS cycle after a single TFS turn. $^{39}K^+$, $^{85}Rb^+$ and $^{133}Cs^+$ ions were then stored for increasing numbers of IT up to 700, 500 and 380 IT inside the analyzer, respectively, corresponding to total time-of-flights of up to 9 ms. In these measurements, data was accumulated for 1000 MR-TOF-MS cycles, corresponding to data accumulation time of 20 s at 50 Hz operation. If accumulated over long times, the peaks experience some additional broadening, due to drifts. Thus, the results shown in Fig 7 represent a conservative performance estimate.

At low numbers of IT the mass resolving power, which was determined from a Gaussian fit, increases linearly with the number of turns. A mass resolving power of 100 000 FWHM, sufficient to resolve most short-lived nuclei, is reached after about 100 IT, corresponding to total time of flights of approximately 1.3, 1.9 and 2.3 ms for $^{39}K^+$, $^{85}Rb^+$ and $^{133}Cs^+$, respectively. This further highlights the advantage of the TFS + IT operational scheme [63], as it creates a time focus at the detector after every full turn. The resolving power increases further with increasing number of IT, but the slope starts to flatten due to aberrations broadening the peaks. The data in Fig. 7 was fitted with eq. 7. All parameters, except the peak broadening per IT Δt_{IT}, were measured directly for the individual species and kept fixed during the fitting. The resolving power can be well described by eq. 7 with only one free parameter. In all cases a mass resolving power exceeding 250 000 FWHM can be reached, despite the rather long data accumulation time of 20 s. Particularly at more than 300 IT, drifts and instabilities on the time scale of a few seconds start to limit the resolving power of the device. The measured resolving power shows much stronger fluctuations at higher number of IT, which can be seen as an indication that the performance is limited by instabilities rather than the ion optical properties of the time-of-flight analyzer. These drifts are caused by fluctuations and instabilities of the potentials applied to the mirror electrodes.

To quantify the dependence of the mass resolving power on the data accumulation time, the resolving power was determined for $^{85}Rb^+$ ions at 500 IT for different data accumulation times, shown in Fig. 8. Accumulating for 1000 individual MR-TOF-MS cycles reproduces the performance shown in Fig. 7. However, shortening the accumulation time allows for more than 50% higher mass resolving power to be reached with the TITAN MR-TOF-MS at same number of IT. In the presence of a sufficiently abundant calibration species, either isobaric or non-isobaric, short accumulation times can be used and, thus, drifts can be corrected for by performing a time-resolved calibration [28]. This allows the device to reach high mass resolving powers (above 400 000 [69]) even during long overall measurements. In the future we expect additional gains from operation with longer cycle times, which will extend the maximal number of IT for a given ion species beyond the current limitations.

3.3. Mass Accuracy

To investigate the mass accuracy and precision of the device isobars at mass 40 u were used. $^{40}Ar^+$ was provided by the OLIS plasma ion source and merged with $^{40}Ca^+$ and $^{40}K^+$

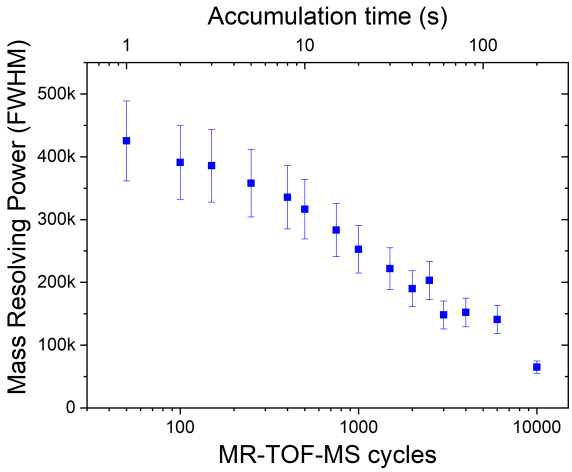

Figure 8: Mass resolving power (FWHM) of $^{85}Rb^+$ ions undergoing 500 isochronous turns as a function of the accumulated MR-TOF-MS cycles (bottom horizontal axis) and corresponding accumulation time (top horizontal axis). At short accumulation times mass resolving powers up to 400 000 have been achieved.

ions from the MR-TOF-MS internal calibration ion source. The ions were stored for 650 IT in the time-of-flight analyzer, corresponding to a total time-of-flight of about 8.1 ms. Data was taken for 3 min with an accumulation time of 2 s. The well-separated peak of $^{40}K^+$ was used for a time resolved calibration. In order to allow for sufficient statistics, the calibration parameter b of eq. 6 was redetermined every 10 s. A mass resolving power of about 300 000 FWHM was reached. During the measurement, the mass range selector was used during the first 30 IT to remove ion species with a different mass number, ensuring an unambiguous mass spectrum. An example time-of-flight spectrum is shown in Fig. 9a. The individual peaks are mostly described by a single Gaussian line shape. However, below 5 – 10% of the peak height the peak shape starts to differ from the Gaussian line shape. For the full description of the line shapes of MR-TOF-MS a so-called Hyper-EMG line shape [70] (a convolution of a Gaussian with exponential functions) can be used. For the TITAN MR-TOF-MS the advantages of a Hyper-EMG line shape have been discussed in [35, 69, 71] and a relative mass accuracies of better than 10^{-7} were demonstrated even for overlapping peaks.

During mass measurements systematic shifts may occur when the ion of interest and the calibration ion species experience different electric fields. This can happen during the ejection from the injection trap, during switching of the analyzer potentials or the mass range selector, or it can be caused by dead-time effects at the detector [51], ion-ion interaction during long time-of-flights or due to a large mass difference between the ion of interest and the calibration species. The later will be discussed in detail in a forthcoming publication.

The single largest contribution to the systematic uncertainty, for mass measurements with an isobaric calibration ion species, is the switching of the second ion mirror to release the ions towards the detector. Assuming a non-ideal switching, the cal-

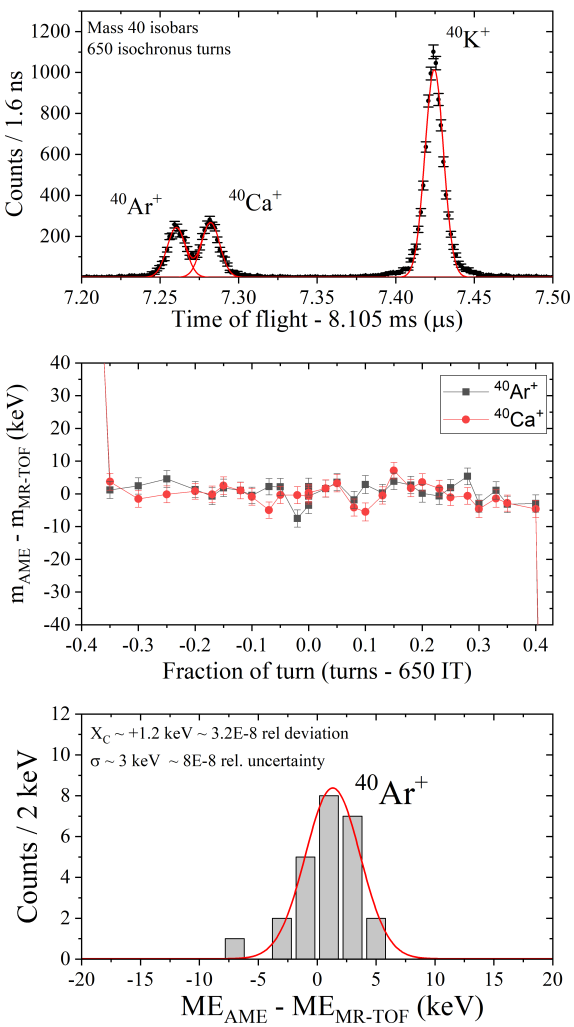

Figure 9: (Top panel) Time-of-flight spectrum of isobars at mass 40 u after 650 isochronous turns, corresponding to about 8 ms total time of flight. Data was taken for 3 minutes. (Middle panel) Variation of the mass values of ^{40}Ar and ^{40}Ca as a function of the time of switching of the 2nd mirror prior to the detection of the ion species. The horizontal axis has been converted from time into units of turns at mass 40 u, indicating a ±35% fraction of the time-of-fight analyzer in which species are not effected by switching of the mirror potentials. (Bottom panel) Scatter of the measured mass of ^{40}Ar determined from the scan shown in the middle panel.

ibration ions may probe different fields compared to the ion of interest, which may alter the time of flight of one of the ion species. Under normal conditions, the second mirror is switched while the ion of interest is turning around in the first mirror, ensuring a maximal distance to the time-varying fields. To quantify this effect, the isobaric triplet at mass 40 u was stored for slightly different times inside the analyzer, effectively probing different distances to the second ion mirror at the moment of switching. The result is shown in Fig. 9 (middle panel), where the time of switching of the second mirror has been converted into fractions of a full IT. Under ideal switching conditions the respective time of flight of the different ion species and therefore the resulting mass values do not change. This can be seen for the region ±35% of the full turn setting. At the edges of the scan, either the ^{40}K$^+$ or the ^{40}Ar$^+$ and ^{40}Ca$^+$ ions probe time-varying electric fields.

The scatter of the resulting ^{40}Ar mass values obtained from the ±35% region is shown in Fig. 9 (bottom panel). The results reproduce the literature mass value with an average deviation of only +1.2 ± 0.7 keV, corresponding to relative deviation of $\Delta m/m \approx 3.2 \times 10^{-8}$, and scatter of $\sigma = 3$ keV, corresponding to $\delta m/m \approx 8 \times 10^{-8}$. A similar result is obtained for ^{40}Ca, whose literature mass can be reproduced within -0.5 ± 0.6 keV and scatter of $\sigma = 2.6$ keV. The mass results for ^{40}Ar and ^{40}Ca deviate by about 1.7 σ and 0.8 σ from their respective literature mass values, which indicates a remaining systematic uncertainty of the TITAN MR-TOF-MS on the order of ≈ 1 keV or $\delta m/m \approx 3 \times 10^{-8}$ for isobaric calibration species.

In summary, the TITAN MR-TOF-MS demonstrates excellent mass accuracy and precision and is capable of performing mass measurements for nuclear structure and astrophysics implications with relative mass accuracies below $\delta m/m < 1\times10^{-7}$.

3.4. Long-Term Stability

To take full advantage of the capabilities of the TITAN MR-TOF-MS during mass measurements of radioactive isotopes, produced at minute quantities, the device has to be capable of operating stably over many hours.

To estimate the stability and the detection limit of the device a long-term measurement with stable potassium ions was performed. All three naturally occurring isotopes, ^{39}K$^+$, ^{40}K$^+$ and ^{41}K$^+$, were injected into the time-of-flight analyzer and stored for 400, 395 and 390 IT, respectively. This resulted in total times of flight of about ≈ 4.9 ms. The intensity of ^{39}K$^+$ was adjusted to a rate of about 2 detected ions per second. Data was accumulated for 87 hours in total, while for individual spectra data was collected for 240 s each. In Fig. 10 (bottom panel) the time of flight of ^{39}K$^+$ is shown throughout the measurement. The overall fluctuations are smooth, but a clear day-and-night drift with a maximal shift of about 120 ns can be seen. The drift corresponds to a temperature change in the ISAC I experimental hall of about 5 K from night to day. A temperature coefficient of ≈ 10 ppm/K for mass measurements with the TITAN MR-TOF-MS can be deduced. However, the comparable slow temperature drifts, with a maximal slope of 27 ns/h, roughly ≈ 11 ppm/h, can effectively be corrected with the time-resolved calibration procedure.

3.5. Sensitivity

The capability to detect minute quantities of an ion species of interest can be estimated based on the above data. In Fig. 10 (top panel) the time-resolved calibrated time-of-flight spectrum is shown. In the spectrum, two small peaks emerge at about 6.8 μs after switching of the second ion mirror. Based on a calibration via eq. 6 they are identified as ^{40}K$^+$ and ^{40}Ca$^+$, detected with rates of 0.7 ± 0.09 and 0.3 ± 0.06 ions per hour, respectively. The measured intensity of ^{40}K$^+$ matches the expected rate of 0.8 ions per hour based on the natural abundance of ^{40}K of only 0.0117(1)% and the detected ^{39}K$^+$ intensity. Furthermore, the detection of minute traces of ^{40}Ca$^+$ from the thermal

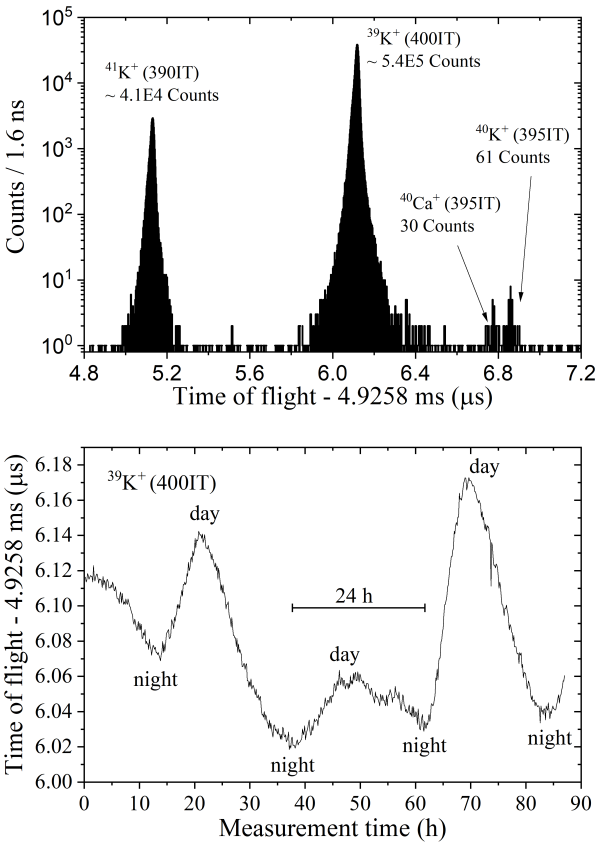

Figure 10: (Top panel) Time-of-flight spectra of natural potassium ^{39}K, ^{40}K and ^{41}K ions undergoing 400, 395 and 390 isochronous turns, respectively. In the measurement ^{39}K was detected at a rate of ≈ 2 ions per second. Spectra were accumulated over 87 hours, each spectra was accumulated for 240 s. In total 61 counts of ^{40}K were detected, in line with the natural abundance of 0.0117%. A mass resolving power of 140 000 was reached after a time-resolved calibration. (bottom panel) Time of flight of $^{39}K^+$ through out the measurement. A 24 hour / day-night period is indicated by the marker.

ion source in relation to the huge $^{39}K^+$ peak indicates a dynamic range of at least 1 to 1.8×10^4. Being able to detect ion species at such low intensities illustrates the excellent sensitivity and dynamic range of the TITAN MR-TOF-MS.

Taking a total efficiency of about ≈ 15% into account, it becomes evident that the TITAN MR-TOF-MS is well capable of performing mass measurements of extremely low count rates. Isotopes produced at rates as low as 10 particles per hour are in reach. To date, the lowest-yield species successfully measured with the TITAN MR-TOF-MS has been ^{105}Sr [72], which was extracted from the ISAC target at a rate of only about ≈ 140 particles per hour (ISAC yield 0.04 particles per second [73]).

4. Performance in Isobar Separation Mode

Many radioactive beam experiments at ISAC are not limited by the available amount of the isotope of interest, but rather by the overwhelming presence of unwanted contaminants and the dynamic range of the mass spectrometer. To suppress unwanted isobaric contamination the TITAN MR-TOF-MS relies on mass selective re-trapping of the ion of interest in the injection trap [58]. Re-trapping was commissioned using stable beams at mass 28 u from the OLIS plasma ion source. The composition of the beam is shown in Fig. 11(top panel) after undergoing 40 IT in the MR-TOF-MS. All components of the beam, such as $^{28}Si^+$, $^{12}C^{16}O^+$, $^{14}N_2{}^+$, $^{12}C^{14}NH_2{}^+$, $^{12}C^{13}CH_3{}^+$ and $^{12}C_2H_4{}^+$, are clearly resolved and have been identified by their respective mass-to-charge ratio.

The MR-TOF-MS was then switched into re-trapping mode. Ions were prepared and injected into the time-of-flight analyzer as in the mass measurement mode, but after 40 IT, the first ion mirror was opened instead of the second and the ions approaching the injection trap were selectively captured. The captured ion species were then stored in the injection trap for 9 ms, until the end of the 10 ms sub-cycle, before being re-injected into the time of flight analyzer for a second analysis. Here, in both operation modes 40 IT were used, but due to the TFS + IT scheme the number of turns used for separation and mass measurement respectively can be chosen independently.

The time between ion injection into the time-of-flight analyzer and re-capture in the injection trap, the so-called re-trapping time, was scanned between 439.9 μs and 440.5 μs, while measuring the composition of the re-captured ions in the consecutive mass measurement cycle. Fig. 11(middle panel) shows a two-dimensional graph of the scan of the re-trapping time. One can see that different ion species are selected at different re-trapping times. Choosing a fixed re-trapping time of 440.14 μs fully isolates $^{12}C^{16}O^+$ from all other species in the beam, as shown in Fig. 11(bottom panel). The mass resolving power in isobar separation mode (mass separation power) can be determined from the width of the capture scan. In this measurement a mass resolving power of 5000 was reached in isobar separation mode using a 10 V deep trapping potential and 40 000 in the mass measurement mode after 40 IT.

The maximal dynamic range of the suppression was investigated by increasing the incoming overall beam intensity until unwanted ion species started to show up in the consecutive mass spectrum. Up to ~ 10^7 incoming ions per second, corresponding to about ~ 10^4 ions per MR-TOF-MS cycle, a suppression of four orders of magnitude could be achieved. At even higher beam intensities the suppression seems to reduce, but was not further investigated in order to not damage the TOF detector in the MR-TOF-MS.

4.1. Efficiency

In isobar separation mode, the efficiency depends on the number of IT, as in the regular mass measurement mode (see section 3.1), and on the capture efficiency of the injection trap. While ion bunches are always prepared in a 15 V deep axial trapping potential, the re-trapping can be made more selective using shallower re-trapping potentials, but that may come at the costs of lower efficiency, see the discussion in [58].

To investigate this behaviour and choose a suitable compromise between re-trapping efficiency and selectivity, re-trapping was measured for different numbers of IT and trap depths, shown in Fig. 12. The efficiency was determined by comparing the intensity between performing only a mass measurement

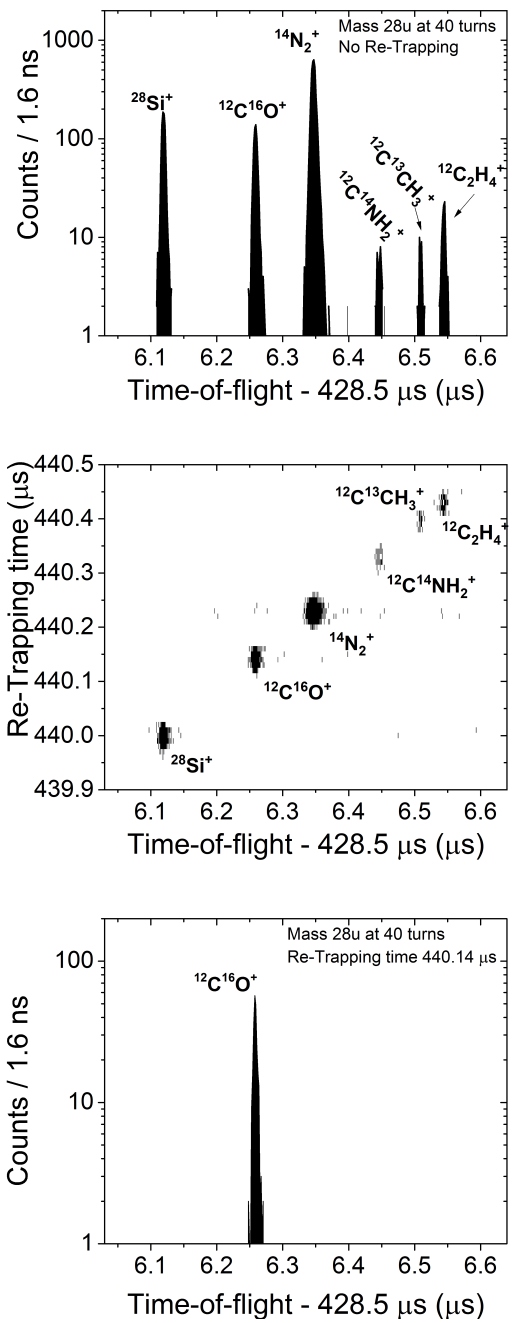

Figure 11: Isobar separation via mass-selective re-trapping with stable beam from ISAC. The ions underwent 40 isochronous turns before being re-trapped in the injection trap. The captured ions were re-cooled and then injected into the mass analyzer for 40 isochronous turns before impinging on the time-of-flight detector. (top panel) Time-of-flight spectra without re-trapping. (middle panel) 2d plot of time-of-flight of the ions in dependence of the re-trapping time. (bottom panel) Example of a time-of-flight spectrum of an ion sample using a fixed re-trapping time of 440.14 μs. Spectra in the top and bottom panel were not accumulated for the same time.

cycle and performing re-trapping and mass measurement consecutively for the same ion population. In this measurement ions were stored for the same number of IT in both cycles. It becomes evident, that for a trap depth exceeding about $\approx$ 5.5 V a plateau in efficiency of about $\approx$ 70% is reached. For lower trapping depth the efficiency of the re-trapping operation drops to around 25% at 3 V trap depth. A small residual fluctuation of the re-trapping efficiency on the number of IT can be observed, it results from imperfect alignment between the beam axis and the ion optical axis of the time-of-flight analyzer. For a given number of IT the re-trapping efficiency can be optimized by adjusting the steering voltages between the injection trap and the time-of-flight analyzer by about 10 V. This procedure was not performed during the above measurement.

4.2. Mass Separation Power

In general, the achievable mass resolving power in isobar separation mode depends on the time-of-flight separation and the selective re-trapping of the injection trap, as described in [58]. The overall separation power is limited by the lower of the two.

Thus, using mass selective re-trapping one can use different strategies to increase the separation power of the device, either by increasing the number of IT or by decreasing the trapping depth used for re-trapping.

The achievable mass separation power was determined as a function of number of turns and trap depth. The results are shown in Fig. 13. The contours show combinations of operational settings, that result in the same resolving power. The combination of shallow trapping potential and high number of turns allows for isobar separation with highest resolving powers, up to 100000 FWHM at 320 IT and 3.2 V trap depth. Under these conditions an efficiency of $\sim$ 15% is reached, see Fig. 12. Employing trap depths above 5.5 V, so highest efficiency, resolving powers up to 40000 FWHM can be reached after 300 IT.

However, typical scans of the re-trapping time show a flat-top behaviour when scanning over the characteristic region of the ion of interest. The edges of the distribution are commonly much sharper compared to the FWHM. Therefore, the edge of the capture distribution can be used to separate close-lying isobars, while maintaining the high efficiency of using a deeper trap, as discussed in [58]. For the TITAN MR-TOF-MS in this edge-separation mode mass separation powers are typically a factor of 2 to 3 higher compared to the FWHM separation at the same trap depth. Considering that typical stable contaminants tend to have lower mass excesses compared to the more exotic isobars of interest, this mode has dominantly been used during online experiments as it allows for high efficiency and high separation power.

Employing re-trapping the dynamic range of the TITAN MR-TOF-MS is enhanced and online mass measurements with ion of interest to contaminant ratios of 1 to 10^6 have been achieved already. Since the first online application of mass selective re-trapping in [74], it has been employed routinely [32, 72]. In the future applying multiple re-trapping cycles before each mass measurement cycle may enhance the dynamic range even further. In addition employing re-trapping at even higher numbers of IT will enable the separation between nuclear isomeric and ground states and allow for isomerically purified ion ensembles.

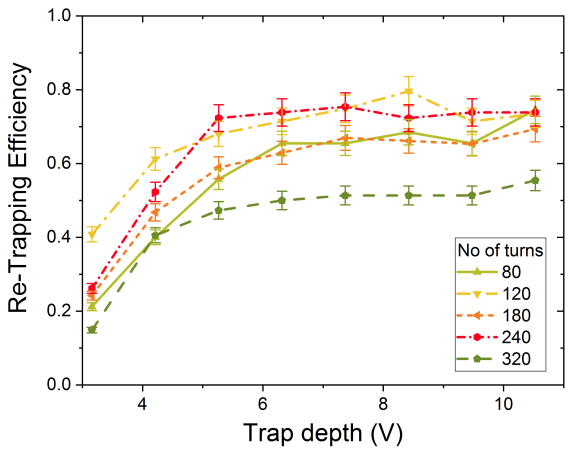

Figure 12: Re-trapping efficiency measured for ^{133}Cs for different numbers of isochronous turns as a function of the re-trapping trap depth. For deeper trapping potentials more ions can be captured until a plateau is reached at about 5.5 V.

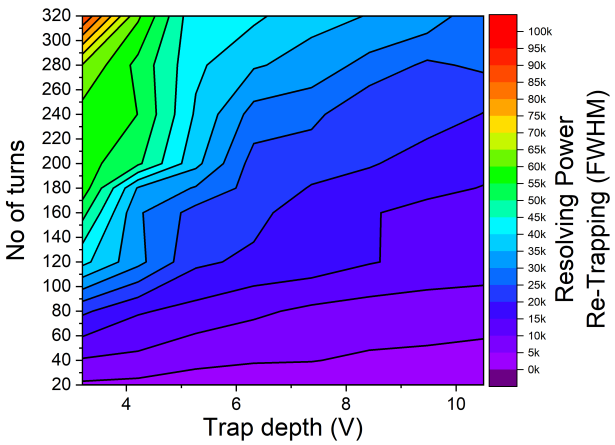

Figure 13: Contour plot showing the measured resolving power in re-trapping mode as a function of number of isochronous turns and trap depth. A resolving power of 100 000 FWHM is reached after 320 isochronous turns at a trap depth of 3.2 V.

In the near future the TITAN MR-TOF-MS will be used for isobar separation for the Measurement Penning Trap MPET or the Electron Beam Ion Trap EBIT and will play a crucial part in TITAN's push towards measurements of more exotic isotopes.

5. Conclusion and Outlook

The TITAN MR-TOF-MS has been successfully commission and since been in routine operation during various experiments at TITAN [24, 25, 26, 35, 21, 69, 67, 32, 72, 74]. The device reaches a high mass resolving power ($m/\Delta m \sim 400\,000$), high precision and mass accuracy (δm /m $< 10^{-7}$), is fast (common measurement cycle time of 20 ms), shows high sensitivity and very strong background handling capabilities (ratios of the ions of interest to the contaminant ions of up to 1 to 10^6). The device can be used to perform high precision mass measurements of short lived radioactive isotopes or provide crucial background suppression by four orders of magnitude for the Measurement Penning Trap MPET or the Electron Beam Ion Trap EBIT. The high mass resolving power makes the device well suitable to cope with highly contaminated beams common to the ISOL radioactive beam production method. The MR-TOF-MS is efficient and, as such, capable of tackling the most exotic nuclei produced at ISAC. Due to the unique combination of mass measurement and isobar separation, using mass selective re-trapping, the TITAN MR-TOF-MS is able to perform mass measurements of isotopes produced well below 1 particle per second out of strong isobaric background with intensities up to 10^6 particles per second. Isotopes extracted from the production target with rates as low as 0.04 particles per second have successfully been measured [72]. Therefore the TITAN MR-TOF-MS allows investigating even more exotic nuclei for nuclear structure studies and with importance to astrophysical processes and enables TITAN to expand its research towards the limits of the nuclear chart.

Acknowledgement

We would like to thank the whole TITAN Collaboration for their support of the MR-TOF-MS project, M. Good for great technical assistance and the ISAC OLIS team for providing colorful stable beams for the commissioning of the MR-TOF-MS. This work is supported in part by the Natural Sciences and Engineering Research Council of Canada (NSERC), the Canada Foundation for Innovation (CFI), the Brazilian Conselho Nacional de Desenvolvimento Científico e Technológico (CNPq) under grant 249121/2013-1, the Helmholtz Association of German Research Centers through the Nuclear Astrophysics Virtual Institute (VH-VI-417), Justus-Liebig-Universität Gießen and GSI under the JLU-GSI strategic Helmholtz partnership agreement, the Hessian Ministry for Science and Art (HMWK) through the LOEWE Center HICforFAIR, the US National Science Foundation under Grant PHY-1419765, the Deutsche Forschungsgemeinschaft (DFG) under Grants FR 601/3-1 and SCHE 1969/2-1, and the German Federal Ministry for Education and Research (BMBF) under Contracts No. 05P16RGFN1, 05P19RGFN1 and 05P21RGFN1. TRIUMF receives federal funding via the National Research Council of Canada (NRC).

[1] Blaum K, Litvinov YA. 100 years of mass spectrometry. International Journal of Mass Spectrometry 2013;349-350:1 – 2. URL: http://www.sciencedirect.com/science/article/pii/S1387380613002704. doi:https://doi.org/10.1016/j.ijms.2013.07.005; 100 years of Mass Spectrometry.

[2] Dilling J, Blaum K, Brodeur M, Eliseev S. Penning-trap mass measurements in atomic and nuclear physics. Annual Review of Nuclear and Particle Science 2018;68(1):45–74. URL: https://doi.org/10.1146/annurev-nucl-102711-094939. doi:10.1146/annurev-nucl-102711-094939. arXiv:https://doi.org/10.1146/annurev-nucl-102711-094939.

[3] Yamaguchi T, Koura H, Litvinov Y, Wang M. Masses of exotic nuclei. Progress in Particle and Nuclear Physics 2021;:103882URL: https://www.sciencedirect.com/science/article/pii/S0146641021000363. doi:https://doi.org/10.1016/j.ppnp.2021.103882.

[4] Dilling J, Bricault P, Smith M, Kluge HJ. The proposed TITAN facility at ISAC for very precise mass measurements on highly charged short-lived isotopes. In: Nucl. Instruments Methods Phys. Res.

Sect. B Beam Interact. with Mater. Atoms; vol. 204. 2003, p. 492–6. URL: http://www.sciencedirect.com/science/article/pii/S0168583X02021183. doi:10.1016/S0168-583X(02)02118-3.

[5] Smith M, Brodeur M, Brunner T, Ettenauer S, Lapierre A, Ringle R, et al. First penning-trap mass measurement of the exotic halo nucleus Li11. Phys Rev Lett 2008;101(20):5–8. URL: http://link.aps.org/doi/10.1103/PhysRevLett.101.202501. doi:10.1103/PhysRevLett.101.202501. arXiv:0807.1260.

[6] Gallant AT, Alanssari M, Bale JC, Andreoiu C, Barquest BR, Chowdhury U, et al. Mass determination near N=20 for Al and Na isotopes. Phys Rev C 2017;96(2):1–5. doi:10.1103/PhysRevC.96.024325.

[7] Bentley I, Rodríguez YC, Cunningham S, Aprahamian A. Shell structure from nuclear observables. Phys Rev C 2016;93(4):044337. URL: https://link.aps.org/doi/10.1103/PhysRevC.93.044337. doi:10.1103/PhysRevC.93.044337. arXiv:arXiv:1604.08143v1.

[8] Horowitz CJ, Arcones A, Côté B, Dillmann I, Nazarewicz W, Roederer IU, et al. r-process nucleosynthesis: connecting rare-isotope beam facilities with the cosmos. Journal of Physics G: Nuclear and Particle Physics 2019;46(8):083001. URL: https://doi.org/10.1088%2F1361-6471%2Fab0849. doi:10.1088/1361-6471/ab0849.

[9] Blumenfeld Y, Nilsson T, Duppen PV. Facilities and methods for radioactive ion beam production. Physica Scripta 2013;T152:014023. URL: https://doi.org/10.1088%2F0031-8949%2F2013%2Ft152%2F014023. doi:10.1088/0031-8949/2013/t152/014023.

[10] Cameron AE, Eggers DF. An ion velocitron. Review of Scientific Instruments 1948;19(9):605–7. URL: https://doi.org/10.1063/1.1741336. doi:10.1063/1.1741336.

[11] Wiley WC, McLaren IH. Time-of-Flight Mass Spectrometer with Improved Resolution. Rev Sci Instrum 1955;26(12):1150. doi:10.1007/s13398-014-0173-7.2.

[12] Wollnik H, Przewloka M. Time-of-flight mass spectrometers with multiply reflected ion trajectories. Int J Mass Spectrom Ion Process 1990;96(3):267–74. doi:10.1016/0168-1176(90)85127-N.

[13] Plass WR, Dickel T, Scheidenberger C. Multiple-reflection time-of-flight mass spectrometry. Int J Mass Spectrom 2013;349-350(1):134–44. URL: http://dx.doi.org/10.1016/j.ijms.2013.06.005. doi:10.1016/j.ijms.2013.06.005.

[14] Wolf RN, Wienholtz F, Atanasov D, Beck D, Blaum K, Borgmann C, et al. ISOLTRAP's multi-reflection time-of-flight mass separator/spectrometer. Int J Mass Spectrom 2013;349-350(1):123–33. URL: http://dx.doi.org/10.1016/j.ijms.2013.03.020. doi:10.1016/j.ijms.2013.03.020.

[15] Schury P, Wada M, Ito Y, Arai F, Naimi S, Sonoda T, et al. A high-resolution multi-reflection time-of-flight mass spectrograph for precision mass measurements at RIKEN/SLOWRI. Nucl Instruments Methods Phys Res Sect B Beam Interact with Mater Atoms 2014;335:39–53. URL: http://dx.doi.org/10.1016/j.nimb.2014.05.016. doi:10.1016/j.nimb.2014.05.016.

[16] Dickel T, Plass WR, Becker A, Czok U, Geissel H, Haettner E, et al. A high-performance multiple-reflection time-of-flight mass spectrometer and isobar separator for the research with exotic nuclei. Nucl Instruments Methods Phys Res Sect A Accel Spectrometers, Detect Assoc Equip 2015;777:172–88. URL: http://dx.doi.org/10.1016/j.nima.2014.12.094http://linkinghub.elsevier.com/retrieve/pii/S0168900214015629. doi:10.1016/j.nima.2014.12.094.

[17] Hirsh TY, Paul N, Burkey M, Aprahamian A, Buchinger F, Caldwell S, et al. First operation and mass separation with the CARIBU MR-TOF. Nucl Instruments Methods Phys Res Sect B Beam Interact with Mater Atoms 2016;376:229–32. URL: http://dx.doi.org/10.1016/j.nimb.2015.12.037. doi:10.1016/j.nimb.2015.12.037.

[18] Chauveau P, Delahaye P, De France G, El Abir S, Lory J, Merrer Y, et al. Pilgrim, a multi-reflection time-of-flight mass spectrometer for spiral2-s3 at ganil. Nuclear Instruments and Methods in Physics Research Section B: Beam Interactions with Materials and Atoms 2016;376:211 –5. URL: http://www.sciencedirect.com/science/article/pii/S0168583X16000732. doi:https://doi.org/10.1016/j.nimb.2016.01.025; proceedings of the XVIIth International Conference on Electromagnetic Isotope Separators and Related Topics (EMIS2015), Grand Rapids, MI, U.S.A., 11-15 May 2015.

[19] Atanasov D, Ascher P, Blaum K, Cakirli RB, Cocolios TE, George S, et al. Precision mass measurements of $^{129--131}$Cd and their impact on stellar nucleosynthesis via the rapid neutron capture process. Phys Rev Lett 2015;115:232501. URL: https://link.aps.org/doi/10.1103/PhysRevLett.115.232501. doi:10.1103/PhysRevLett.115.232501.

[20] Orford R, Vassh N, Clark JA, McLaughlin GC, Mumpower MR, Savard G, et al. Precision mass measurements of neutron-rich neodymium and samarium isotopes and their role in understanding rare-earth peak formation. Phys Rev Lett 2018;120:262702. URL: https://link.aps.org/doi/10.1103/PhysRevLett.120.262702. doi:10.1103/PhysRevLett.120.262702.

[21] Reiter MP, Ayet San Andrés S, Nikas S, Lippuner J, Andreoiu C, Babcock C, et al. Mass measurements of neutron-rich gallium isotopes refine production of nuclei of the first *r*-process abundance peak in neutron-star merger calculations. Phys Rev C 2020;101:025803. URL: https://link.aps.org/doi/10.1103/PhysRevC.101.025803. doi:10.1103/PhysRevC.101.025803.

[22] Wienholtz F, Beck D, Blaum K, Borgmann C, Breitenfeldt M, Cakirli RB, et al. Masses of exotic calcium isotopes pin down nuclear forces. Nature 2013;498(7454):346–9. URL: http://www.nature.com/doifinder/10.1038/nature12226. doi:10.1038/nature12226.

[23] Rosenbusch M, Ascher P, Atanasov D, Barbieri C, Beck D, Blaum K, et al. Probing the N=32 Shell Closure below the Magic Proton Number Z=20: Mass Measurements of the Exotic Isotopes K. Phys Rev Lett 2015;114(20). URL: http://journals.aps.org/prl/abstract/10.1103/PhysRevLett.114.202501. doi:10.1103/PhysRevLett.114.202501. arXiv:1506.0520.

[24] Leistenschneider E, Reiter MP, Ayet San Andrés S, Kootte B, Holt JD, Navrátil P, et al. Dawning of the $n = 32$ shell closure seen through precision mass measurements of neutron-rich titanium isotopes. Phys Rev Lett 2018;120:062503. URL: https://link.aps.org/doi/10.1103/PhysRevLett.120.062503. doi:10.1103/PhysRevLett.120.062503.

[25] Reiter MP, Ayet San Andrés S, Dunling E, Kootte B, Leistenschneider E, Andreoiu C, et al. Quenching of the $n = 32$ neutron shell closure studied via precision mass measurements of neutron-rich vanadium isotopes. Phys Rev C 2018;98:024310. URL: https://link.aps.org/doi/10.1103/PhysRevC.98.024310. doi:10.1103/PhysRevC.98.024310.

[26] Leistenschneider E, Dunling E, Bollen G, Brown BA, Dilling J, Hamaker A, et al. (The LEBIT Collaboration and the TITAN Collaboration). Precision mass measurements of neutron-rich scandium isotopes refine the evolution of $n = 32$ and $n = 34$ shell closures. Phys Rev Lett 2021;126:042501. URL: https://link.aps.org/doi/10.1103/PhysRevLett.126.042501. doi:10.1103/PhysRevLett.126.042501.

[27] Rosenbusch M, Ito Y, Schury P, Wada M, Kaji D, Morimoto K, et al. New mass anchor points for neutron-deficient heavy nuclei from direct mass measurements of radium and actinium isotopes. Phys Rev C 2018;97:064306. URL: https://link.aps.org/doi/10.1103/PhysRevC.97.064306. doi:10.1103/PhysRevC.97.064306.

[28] Ayet San Andres S, Hornung C, Ebert J, Plass WR, Dickel T, Geissel H, et al. High-resolution, accurate multiple-reflection time-of-flight mass spectrometry for short-lived, exotic nuclei of a few events in their ground and low-lying isomeric states. Phys Rev C 2019;99:064313. doi:10.1103/PhysRevC.99.064313.

[29] Ito Y, Schury P, Wada M, Arai F, Haba H, Hirayama Y, et al. First direct mass measurements of nuclides around $z = 100$ with a multireflection time-of-flight mass spectrograph. Phys Rev Lett 2018;120:152501. URL: https://link.aps.org/doi/10.1103/PhysRevLett.120.152501. doi:10.1103/PhysRevLett.120.152501.

[30] Dickel T, Plaß W, Ayet San Andres S, Ebert J, Geissel H, Haettner E, et al. First spatial separation of a heavy ion isomeric beam with a multiple-reflection time-of-flight mass spectrometer. Physics Letters B 2015;744:137 –41. URL: http://www.sciencedirect.com/science/article/pii/S0370269315002105. doi:https://doi.org/10.1016/j.physletb.2015.03.047.

[31] Hornung C, Amanbayev D, Dedes I, Kripko-Koncz G, Miskun I, Shimizu N, et al. Isomer studies in the vicinity of the doubly-magic nucleus 100sn: Observation of a new low-lying isomeric state in 97ag. Physics

Letters B 2020;802:135200. URL: http://www.sciencedirect.com/science/article/pii/S0370269320300046. doi:https://doi.org/10.1016/j.physletb.2020.135200.

[32] Izzo C, Bergmann J, Dietrich KA, Dunling E, Fusco D, Jacobs A, et al. Mass measurements of neutron-rich indium isotopes for *r*-process studies. Phys Rev C 2021;103:025811. URL: https://link.aps.org/doi/10.1103/PhysRevC.103.025811. doi:10.1103/PhysRevC.103.025811.

[33] Jesch C. The multiple-reflection time-of-flight isobar separator for titan and direct mass measurements at the frs ion catcher. Ph.D. thesis; Justus-Liebig-Universitaet; 2016. URL: http://geb.uni-giessen.de/geb/volltexte/2016/12096.

[34] Jesch C, Dickel T, Plass WR, Short D, Ayet San Andres S, Dilling J, et al. The MR-TOF-MS isobar separator for the TITAN facility at TRIUMF. Hyperfine Interact 2015;235(1-3):97–106. URL: http://link.springer.com/10.1007/s10751-015-1184-2. doi:10.1007/s10751-015-1184-2.

[35] Dickel T, San Andrés SA, Beck S, Bergmann J, Dilling J, Greiner F, et al. Recent upgrades of the multiple-reflection time-of-flight mass spectrometer at titan, triumf. Hyperfine Interactions 2019;240(1):62.

[36] Dombsky M, Bishop D, Bricault P, Dale D, Hurst A, Jayamanna K, et al. Commissioning and initial operation of a radioactive beam ion source at ISAC. Rev Sci Instrum 2000;71(2):978. URL: http://scitation.aip.org/content/aip/journal/rsi/71/2/10.1063/1.1150364. doi:10.1063/1.1150364.

[37] Ball GC, Hackman G, Krücken R. The TRIUMF-ISAC facility: two decades of discovery with rare isotope beams. Phys Scr 2016;91(9):93002. URL: http://stacks.iop.org/1402-4896/91/i=9/a=093002?key=crossref.fc9ffc9178e75a0a0c964964b041de4a. doi:10.1088/0031-8949/91/9/093002.

[38] Kunz P, Bricault P, Dombsky M, Erdmann N, Hanemaayer V, Wong J, et al. Composite uranium carbide targets at TRIUMF: Development and characterization with SEM, XRD, XRF and L-edge densitometry. J Nucl Mater 2013;440(1-3):110–6. URL: http://dx.doi.org/10.1016/j.jnucmat.2013.04.065. doi:10.1016/j.jnucmat.2013.04.065.

[39] Bricault P, Baartman R, Dombsky M, Hurst A, Mark C, Stanford G, et al. TRIUMF-ISAC target station and mass separator commissioning. Nucl Phys A 2002;701(1-4):49–53. URL: http://linkinghub.elsevier.com/retrieve/pii/S0375947401015469. doi:10.1016/S0375-9474(01)01546-9.

[40] Brunner T, Smith MJ, Brodeur M, Ettenauer S, Gallino R, Simon VV, et al. TITAN's digital RFQ ion beam cooler and buncher, operation and performance. Nucl Instruments Methods Phys Res Sect A Accel Spectrometers, Detect Assoc Equip 2012;676:32–43. URL: http://linkinghub.elsevier.com/retrieve/pii/S0168900212001398. doi:10.1016/j.nima.2012.02.004. arXiv:1107.2187.

[41] Ringle R, Bollen G, Prinke A, Savory J, Schury P, Schwarz S, et al. A "lorentz" steerer for ion injection into a penning trap. International Journal of Mass Spectrometry 2007;263(1):38 – 44. URL: http://www.sciencedirect.com/science/article/pii/S1387380606005781. doi:https://doi.org/10.1016/j.ijms.2006.12.008.

[42] Brodeur M, Ryjkov V, Brunner T, Ettenauer S, Gallant A, Simon V, et al. Verifying the accuracy of the titan penning-trap mass spectrometer. International Journal of Mass Spectrometry 2012;310:20 – 31. URL: http://www.sciencedirect.com/science/article/pii/S1387380611004568. doi:https://doi.org/10.1016/j.ijms.2011.11.002.

[43] Lapierre A, Brodeur M, Brunner T, Ettenauer S, Gallant AT, Simon V, et al. The TITAN EBIT charge breeder for mass measurements on highly charged short-lived isotopes - First online operation. Nucl Instruments Methods Phys Res Sect A Accel Spectrometers, Detect Assoc Equip 2010;624(1):54–64. doi:10.1016/j.nima.2010.09.030.

[44] Leach K, Grossheim A, Lennarz A, Brunner T, Crespo López-Urrutia J, Gallant A, et al. The titan in-trap decay spectroscopy facility at triumf. Nuclear Instruments and Methods in Physics Research Section A: Accelerators, Spectrometers, Detectors and Associated Equipment 2015;780:91 –9. URL: http://www.sciencedirect.com/science/article/pii/S0168900215001023. doi:https://doi.org/10.1016/j.nima.2014.12.118.

[45] Leistenschneider E, Klawitter R, Lennarz A, Alanssari M, Bale JC, Barquest BR, et al. Diversifying beam species through decay and recapture ion trapping: a demonstrative experiment at TITAN-EBIT. Journal of Physics G: Nuclear and Particle Physics 2020;47(4):045113. URL: https://doi.org/10.1088%2F1361-6471%2Fab6ee1. doi:10.1088/1361-6471/ab6ee1.

[46] Dilling J, Baartman R, Bricault P, Brodeur M, Blomeley L, Buchinger F, et al. Mass measurements on highly charged radioactive ions, a new approach to high precision with titan. International Journal of Mass Spectrometry 2006;251(2):198 – 203. URL: http://www.sciencedirect.com/science/article/pii/S1387380606000777. doi:https://doi.org/10.1016/j.ijms.2006.01.044; uLTRA-ACCURATE MASS SPECTROMETRY AND RELATED TOPICS Dedicated to H.-J. Kluge on the occasion of his 65th birthday anniversary.

[47] Lascar D, Klawitter R, Babcock C, Leistenschneider E, Stroberg SR, Barquest BR, et al. Precision mass measurements of $^{125--127}$Cd isotopes and isomers approaching the $n = 82$ closed shell. Phys Rev C 2017;96:044323. URL: https://link.aps.org/doi/10.1103/PhysRevC.96.044323. doi:10.1103/PhysRevC.96.044323.

[48] Babcock C, Klawitter R, Leistenschneider E, Lascar D, Barquest B, Finlay A, et al. Mass measurements of neutron-rich indium isotopes toward the n= 82 shell closure. Physical Review C 2018;97(2):024312.

[49] Plass WR, Dickel T, Andres SSAS, Ebert J, Greiner F, Hornung C, et al. High-performance multiple-reflection time-of-flight mass spectrometers for research with exotic nuclei and for analytical mass spectrometry. Phys Scr 2015;T166(1):014069. URL: http://stacks.iop.org/1402-4896/2015/i=T166/a=014069?key=crossref.e0f68d2f9ebffe242d325f8155dc01f8. doi:10.1088/0031-8949/2015/T166/014069.

[50] Dickel T, Plass WR, Lang J, Ebert J, Geissel H, Haettner E, et al. Multiple-reflection time-of-flight mass spectrometry for in situ applications. Nucl Instruments Methods Phys Res Sect B Beam Interact with Mater Atoms 2013;317(PART B):779–84. URL: http://dx.doi.org/10.1016/j.nimb.2013.08.021. doi:10.1016/j.nimb.2013.08.021.

[51] Andres SAS. Developments for multiple-reflection time-of-flight mass spectrometers and their application to high-resolution accurate mass measurements of short-lived exotic nuclei. Ph.D. thesis; Justus-Liebig-Universitaet; 2018. URL: http://geb.uni-giessen.de/geb/volltexte/2018/13781.

[52] Reiter M, Ames F, Andreoiu C, Ayet San Andrés S, Babcock C, Barquest B, et al. Improved beam diagnostics and optimization at isac via titan's mr-tof-ms. Nuclear Instruments and Methods in Physics Research Section B: Beam Interactions with Materials and Atoms 2020;463:431 –6. URL: http://www.sciencedirect.com/science/article/pii/S0168583X19302186. doi:https://doi.org/10.1016/j.nimb.2019.04.034.

[53] Plass WR, Dickel T, Czok U, Geissel H, Petrick M, Reinheimer K, et al. Isobar separation by time-of-flight mass spectrometry for low-energy radioactive ion beam facilities. Nucl Instruments Methods Phys Res Sect B Beam Interact with Mater Atoms 2008;266(19-20):4560–4. URL: http://dx.doi.org/10.1016/j.nimb.2008.05.079. doi:10.1016/j.nimb.2008.05.079.

[54] Bradbury NE, Nielsen RA. Absolute values of the electron mobility in hydrogen. Phys Rev 1936;49:388–93. URL: https://link.aps.org/doi/10.1103/PhysRev.49.388. doi:10.1103/PhysRev.49.388.

[55] Wolf R, Beck D, Blaum K, Böhm C, Borgmann C, Breitenfeldt M, et al. On-line separation of short-lived nuclei by a multi-reflection time-of-flight device. Nuclear Instruments and Methods in Physics Research Section A: Accelerators, Spectrometers, Detectors and Associated Equipment 2012;686:82 – 90. URL: http://www.sciencedirect.com/science/article/pii/S016890021200575X. doi:https://doi.org/10.1016/j.nima.2012.05.067.

[56] Johnson JT, Carrick IJ, Eakins GS, McLuckey SA. Mirror switching for high-resolution ion isolation in an electrostatic linear ion trap. Analytical chemistry 2019;91(14):8789–94.

[57] Wienholtz F, Kreim S, Rosenbusch M, Schweikhard L, Wolf R. Mass-selective ion ejection from multi-reflection time-of-flight devices via a pulsed in-trap lift. International Journal of Mass Spectrometry 2017;421:285 –93. URL: http://www.sciencedirect.com/science/article/pii/S1387380617301987. doi:https:

//doi.org/10.1016/j.ijms.2017.07.016.

[58] Dickel T, Plass WR, Lippert W, Lang J, Yavor MI, Geissel H, et al. Isobar Separation in a Multiple-Reflection Time-of-Flight Mass Spectrometer by Mass-Selective Re-Trapping. J Am Soc Mass Spectrom 2017;28(6):1079–90. doi:10.1007/s13361-017-1617-z.

[59] Ebert J. Mass Measurements of U-Projectile Fragments for the First Time with a Multiple-Reflection Time-Of-Flight Mass Spectrometer. Ph.D. thesis; Justus-Liebig-Universitaet; 2016. URL: http://geb.uni-giessen.de/geb/volltexte/2016/12170.

[60] Plass WR, Dickel T, Purushothaman S, Dendooven P, Geissel H, Ebert J, et al. The FRS Ion Catcher - A facility for high-precision experiments with stopped projectile and fission fragments. Nucl Instruments Methods Phys Res Sect B Beam Interact with Mater Atoms 2013;317(PART B):457–62. doi:10.1016/j.nimb.2013.07.063.

[61] Haettner E, R. Plaß W, Czok U, Dickel T, Geissel H, Kinsel W, et al. A versatile triple radiofrequency quadrupole system for cooling, mass separation and bunching of exotic nuclei. Nuclear Instruments and Methods in Physics Research Section A: Accelerators, Spectrometers, Detectors and Associated Equipment 2018;880:138 –51. URL: http://www.sciencedirect.com/science/article/pii/S0168900217310409. doi:https://doi.org/10.1016/j.nima.2017.10.003.

[62] Yavor MI, Plass WR, Dickel T, Geissel H, Scheidenberger C. Ion-optical design of a high-performance multiple-reflection time-of-flight mass spectrometer and isobar separator. Int J Mass Spectrom 2015;381-382(1):1–9. URL: http://dx.doi.org/10.1016/j.ijms.2015.01.002. doi:10.1016/j.ijms.2015.01.002.

[63] Dickel T, Yavor MI, Lang J, Plass WR, Lippert W, Geissel H, et al. Dynamical time focus shift in multiple-reflection time-of-flight mass spectrometers. Int J Mass Spectrom 2017;412:1–7. URL: http://dx.doi.org/10.1016/j.ijms.2016.11.005. doi:10.1016/j.ijms.2016.11.005.

[64] Jayamanna K, Ames F, Cojocaru G, Baartman R, Bricault P, Dube R, et al. Off-line ion source terminal for isac at triumf. Review of Scientific Instruments 2008;79(2):02C711. URL: https://aip.scitation.org/doi/abs/10.1063/1.2816928. doi:10.1063/1.2816928. arXiv:https://aip.scitation.org/doi/pdf/10.1063/1.2816928.

[65] Wolf R, Atanasov D, Blaum K, Kreim S, Lunney D, Manea V, et al. Background-free beta-decay half-life measurements by in-trap decay and high-resolution mr-tof mass analysis. Nuclear Instruments and Methods in Physics Research Section B: Beam Interactions with Materials and Atoms 2016;376:275–80. URL: https://www.sciencedirect.com/science/article/pii/S0168583X16001063. doi:https://doi.org/10.1016/j.nimb.2016.01.045; proceedings of the XVIIth International Conference on Electromagnetic Isotope Separators and Related Topics (EMIS2015), Grand Rapids, MI, U.S.A., 11-15 May 2015.

[66] Ayet San Andrés S, Mollaebrahimi A, Dickel T, Bergmann J, Ebert J, Geissel H, et al. Mass and half-life measurements of neutron-deficient iodine isotopes. The European Physical Journal A 2020;56:1–6.

[67] Mukul I, Andreoiu C, Brodeur M, Brunner T, Dietrich K, Dickel T, et al. Measuring the half-life of n-rich 100Rb with the TITAN MR-TOF-MS. Journal of Physics: Conference Series 2020;1643(1):012057.

[68] Kunz P, Andreoiu C, Bricault P, Dombsky M, Lassen J, Teigelhöfer A, et al. Nuclear and in-source laser spectroscopy with the ISAC yield station. Rev Sci Instrum 2014;85(5). doi:10.1063/1.4878718.

[69] Smith MB, Murböck T, Dunling E, Jacobs A, Kootte B, Lan Y, et al. High-precision mass measurement of neutron-rich 96kr. Hyperfine Interactions 2020;241(1):1–8.

[70] Purushothaman S, Ayet San Andrés S, Bergmann J, Dickel T, Ebert J, Geissel H, et al. Hyper-EMG: A new probability distribution function composed of Exponentially Modified Gaussian distributions to analyze asymmetric peak shapes in high-resolution time-of-flight mass spectrometry. Int J Mass Spectrom 2017;421:245–54. URL: https://doi.org/10.1016/j.ijms.2017.07.014. doi:10.1016/j.ijms.2017.07.014.

[71] Paul SF. emgfit - Fitting of time-of-flight mass spectra with hyper-EMG models. 2021. URL: https://doi.org/10.5281/zenodo.4731153. doi:10.5281/zenodo.4731153.

[72] Mukul I, Andreoiu C, Bergmann J, Brodeur M, Brunner T, Dietrich KA, et al. Examining the nuclear mass surface of rb and sr isotopes in the $a \approx 104$ region via precision mass measurements. Phys Rev C 2021;103:044320. URL: https://link.aps.org/doi/10.1103/PhysRevC.103.044320. doi:10.1103/PhysRevC.103.044320.

[73] Kunz P. ISAC Yield Database. 2020. URL: https://mis.triumf.ca/science/planning/yield/beam.

[74] Beck S, Kootte B, Dedes I, Dickel T, Kwiatkowski AA, Lykiardopoulou EM, et al. Mass measurements of neutron-deficient yb isotopes and nuclear structure at the extreme proton-rich side of the $n = 82$ shell. Phys Rev Lett 2021;127:112501. URL: https://link.aps.org/doi/10.1103/PhysRevLett.127.112501. doi:10.1103/PhysRevLett.127.112501.